Journal of Materials Chemistry B

PAPER

View Article Online
View Journal | View Issue

Cite this: J. Mater. Chem. B, 2014, 2, 6397

Tuning the composition of biocompatible Gd nanohydrogels to achieve hypersensitive dual T_1/T_2 MRI contrast agents†

Maité Callewaert,*[a] Valérie Gaëlle Roullin,[a] Cyril Cadiou,[b] Elodie Millart,[ab] Laurence Van Gulik,[c] Marie Christine Andry,[a] Christophe Portefaix,[d] Christine Hoeffel,[d] Sophie Laurent,[e] Luce Vander Elst,[ef] Robert Muller,[ef] Michael Molinari[g] and Françoise Chuburu*[b]

Received 14th May 2014
Accepted 18th July 2014

DOI: 10.1039/c4tb00783b

www.rsc.org/MaterialsB

A series of hydrogel nanoparticles incorporating MRI contrast agents (GdDOTP and MS325) as potential cross-linkers were elaborated by an easy and robust ionotropic gelation process. By this process, high Gd loadings were obtained (between 1.8 and 14.5 × 10^4 Gd centres per NP). By tuning the cross-linker ionization degree and the nature of the polymer matrix it was possible to boost the r_1 relaxivity per Gd centre up to 22-fold. The greatest gains in relaxivity were observed for nanogels for which the polymer matrix was constituted of chitosan and hyaluronan. Relaxivities per Gd centre as high as 100 s^{-1} mM^{-1} at 30 MHz can be reached, which highlighted the fact that molecular motion of the Gd chelate was effectively restricted and water access to the inner core of these nanogels was not limited.

Introduction

Medical imaging techniques nowadays play a central role in clinical diagnoses and for the follow-up after treatment, particularly in an oncological context.[1] Among different imaging modalities, Magnetic Resonance Imaging (MRI) plays a critical role in detection and diagnosis, since it is non-invasive, it does not require the use of ionizing radiation and provides excellent contrast resolution.[2] Contrast tissue in MRI is multifactorial, depending on the imaging sequence and the relaxation time of protons in tissues (longitudinal T_1 and transversal T_2 relaxation times).[2] However, MRI suffers from the lack of sensitivity and information obtained from a simple unenhanced MR image is often not sufficient to highlight the areas of interest. Thus, the contrast has to be improved by administering optimal contrast-enhancing agents (CAs). The most currently used contrast agents are T_1-CAs, constituted of paramagnetic metal ions with symmetrical electronic ground states, such as gadolinium (GdCAs).[3–5] They are used to selectively alter the longitudinal relaxation rates of water protons in the tissues.[3–5] This change in longitudinal relaxation results in a signal intensity increase (positive contrast) of most abnormal tissues and hence facilitates visualization of pathological structures or lesions. To be used under safe conditions for the patients, these metal ions cannot be used as aqua-ions[6,7] but as stable water soluble chelates. The contrast enhancing capacity of a GdCA is quantitatively represented as its relaxivity r_i (units s^{-1} mM^{-1}). The relaxivity, which represents the paramagnetic relaxation rate per mM of Gd(III) (r_i, $i = 1, 2$), is in the range 3–5 s^{-1} mM^{-1} for the currently available GdCAs at 60 MHz. These rather low values imply the injection of GdCAs at high concentrations (>0.1 mmol mL^{-1}) to provide the desired contrast. For the standard clinical applications, these relaxivities are sufficient but the required high Gd doses can be problematic for patients with renal failure.[6,7] Nevertheless, for molecular or cellular imaging, relaxivities have to be improved

[a]Institut de Chimie Moléculaire de Reims, CNRS UMR 7312, Université de Reims Champagne Ardenne, UFR de Pharmacie, 51 rue Cognacq-Jay, 51100 Reims, France. E-mail: maite.callewaert@univ-reims.fr; Tel: +33 326918054

[b]Institut de Chimie Moléculaire de Reims, CNRS UMR 7312, Université de Reims Champagne Ardenne, BP 1039, 51687 Reims Cedex 2, France. E-mail: francoise.chuburu@univ-reims.fr; Tel: +33 326913330

[c]Laboratoire de Pharmacologie, CNRS 3481 MEDyC, UFR Pharmacie, 51095 Reims Cedex, France

[d]Service de Radiologie, CHU de Reims – Hôpital Maison Blanche, 45 Rue Cognacq-Jay, 51092 Reims Cedex, France

[e]Univ. Mons, NMR & Mol. Imaging Lab, Dept Gen Organ & Biomed Chem, B-7000 Mons, Belgium

[f]Center for Microscopy and Molecular Imaging, Rue Adrienne Bolland 8, B-6041 Charleroi, Belgium

[g]Laboratoire de Recherche en Nanosciences, EA4682 Université de Reims Champagne Ardenne, 21 rue Clément Ader, 51685 Reims Cedex 2, France

† Electronic supplementary information (ESI) available: (ESI-1) Evolution of T_1 relaxation rates (40 MHz, 37 °C) for GdDOTP and MS325 in citric acid solution. (ESI-2) Size distribution of GdDOTP⊂NP2 and MS325⊂NP2 from AFM images. (ESI-3) Speciation diagrams of GdDOTP and GdDOTA as a function of pH. (ESI-4) Release profiles of GdDOTP⊂NP1, GdDOTP⊂NP2 and MS325⊂NP2 at 37 °C in phosphate buffer. (ESI-5) Relaxivity calculations. (ESI-6) Comparison of GdDOTP⊂NP1 and GdDOTA⊂NP1 NMRD relaxivity profiles. (ESI-7) a-T_1- and T_2-weighted images at 3 T of GdDOTP⊂NP1. (ESI-8) MTT assay on primary fibroblast cells in the presence of unloaded NPs and Gd⊂NPs. See DOI: 10.1039/c4tb00783b

because the molecular targets are present at much lower concentrations (nano- or picomolar range).[8,9] The Solomon–Bloembergen–Morgan theory[10] (SBM) provides guidelines for the amplification of the r_1 values. For applications at 0.5–1.5 T, high relaxivity (r_1 greater than 100 s^{-1} mM^{-1} per Gd(III) ion) can be achieved by controlling the tumbling motion of the GdCAs and by ensuring optimal water residence times in the gadolinium coordination sphere.[2,11] For this, low molecular weight Gd chelates have been associated through covalent or noncovalent bindings to macro- or supramolecular carriers.[12,13] Nevertheless, high relaxivity values predicted by theory have been seldom achieved because of relatively long residence lifetime of the bound water molecule and of local rotational motions about the linker between the Gd chelate and the anchoring site on the macromolecular backbone.[13] To address these limitations, nano-sized agents integrating Gd chelates including dendrimers,[14] modified natural nanoparticles,[15] auto-assembled systems,[16,17] metal–organic frameworks,[18] fullerenes[19] inorganic nanoparticles[20,21] and nanogels[22,23] have been developed with enhancement in relaxivity in the range of 3 to 10 fold compared to that of the free Gd chelate.

Recently, some examples based on the confinement of Gd chelates within nano-structures such as apoferritine,[24] zeolites,[25] silicon microparticles[26] and silica nanoparticles[27] allowed to pass a milestone in relaxivity enhancement (17 to 50 times larger than that of clinically available GdCAs) and provided a new route to hypersensitive MRI probes. These new nano-constructs observe SBM theory requirements since GdCA confinement within these objects restricts strongly their local rotational motions. Besides this action, water permeability and increase in the effective viscosity of the aqueous solution trapped within the nano-object can contribute to relaxivity.

Biocompatibility of the nanosystems is a crucial issue for MRI clinical applications. In this line, we have recently encapsulated in a hydrophilic matrix, constituted by physical gelation of chitosan (CH) with sodium hyaluronate (HA) and GdDOTA[28] (the GdCA of DOTAREM®) which is recognized as a low-risk CA towards nephrogenic systemic fibrosis (NSF) in patients with renal failure.[6] Either for biocompatibility reasons or for hydrophilic properties, water-soluble chitosan (CH)[29] and sodium hyaluronate (HA)[30] were chosen to constitute the polymer matrix of the nanoparticles. These biopolymers are polycationic polymers (CH), composed of *N*-acetylglucosamine and glucosamine residues and polyanionic polymers (HA), composed of glucuronic acid and *N*-acetylglucosamine residues. They can associate randomly in solution through multivalent ionic interactions[31] into supramolecular architectures which are able to boost the relaxivity of GdDOTA.[28] Indeed, at 60 MHz and 37 °C the relaxivities r_1 and r_2 were 72.3 s^{-1} mM^{-1} and 177.5 s^{-1} mM^{-1} respectively (*i.e.* 24 times higher for r_1 and 52 times higher for r_2 compared to the free complex). Based on this concept, several variations can be envisaged in the hydrogel architecture. The physical chitosan gelation can be modulated through parameters such as pH,[32] presence of additional small anionic species or cross-linkers[33,34] or constitution of a single or an hybrid polymer network. Particularly, one can envisage that anionic GdCAs could themselves act as cross-linkers in the process. Moreover, the nano-hydrogel water content could be tuned according to the composition of the polymer network. To have an insight into these aspects, we compare in this work two different approaches to incorporate GdCAs by physical gelation within chitosan nanoparticles (NPs). For this purpose, CH nano-hydrogels were constituted either of a single polymer network (CH) or of an hybrid polymer network (polyelectrolyte complexes of CH and HA)[28] (Scheme 1). In addition to their potential utility as GdCAs, multi-valent anions GdDOTP (ref. 35) and MS325 (ref. 36) (Scheme 1) were chosen for their ability to act as possible anionic cross-linking agents through their phosphonate functions. Indeed, negative charges localized on the oxygen atoms of the phosphonate groups directed outwards from the Gd coordination cage could favor multiple electrostatic interactions and formation of strong ion-pairs[37,38] within the polymer network. The objective of this study was first to identify the respective roles of HA and GdCAs in the elaboration of the hydrogel network. Secondly, we wished to examine the incidence of the nanohydrogel composition on the relaxivities r_1 and r_2 of the corresponding GdCA loaded nanoparticles.

Results and discussion

Syntheses of nanoparticles

In the first protocol, NP formation was provoked by addition of 1 M NaOH solution to CH solubilised in a citric acid solution. Gadolinium-loaded NPs (GdCA⊂NPs) were prepared using the same procedure, by incorporating GdDOTP or MS325 in the CH phase (Scheme 1, protocol 1 and GdCA⊂NP1 nanoparticles). In the second protocol, CH solubilised in a citric acid solution was allowed to react with polyanions (HA and sodium tripolyphosphate TPP). The formation of polyelectrolyte complexes through electrostatic interactions between polycationic CH and polyanions induced the gelation process.[28,39] Gadolinium-loaded NPs were prepared in the same way, by incorporating GdDOTP or MS325 in the polyanion phase (Scheme 1, protocol 2 and GdCA⊂NP2). For GdDOTP, nanoparticles were obtained for each protocol. For MS325, only protocol 2 gave nanoparticles while for protocol 1 flocculation was observed as soon as MS325 was poured in the acidic CH phase. Since in protocol 1 GdCAs were introduced in the citric acid phase, the stabilities of Gd chelates under acidic conditions were analysed by ^{1}H relaxometry for one day (ESI-1†). Under these conditions, for GdDOTP, 80% of the initial longitudinal relaxation time was still maintained after 12 h. One should then consider that GdDOTP remained intact throughout the encapsulation process. In contrast, the longitudinal relaxation time of MS325 rapidly collapsed to reach the relaxation time of the Gd(III) ion. It indicated that, in acidic medium, MS325 was rapidly demetalated. This result could account for the inability to obtain MS325⊂NPs with protocol 1. On the other hand, since in protocol 2 MS325 was added in the polyanion phase, acidic conditions were avoided and then NPs were recovered.

The GdCA⊂NPs were then purified by dialysis (GdDOTP⊂NPs) or by gel permeation (MS325⊂NPs) and concentrated, when necessary, by tangential filtration. For dialyzed nanoparticles, one should notice that, upon dialysis, the

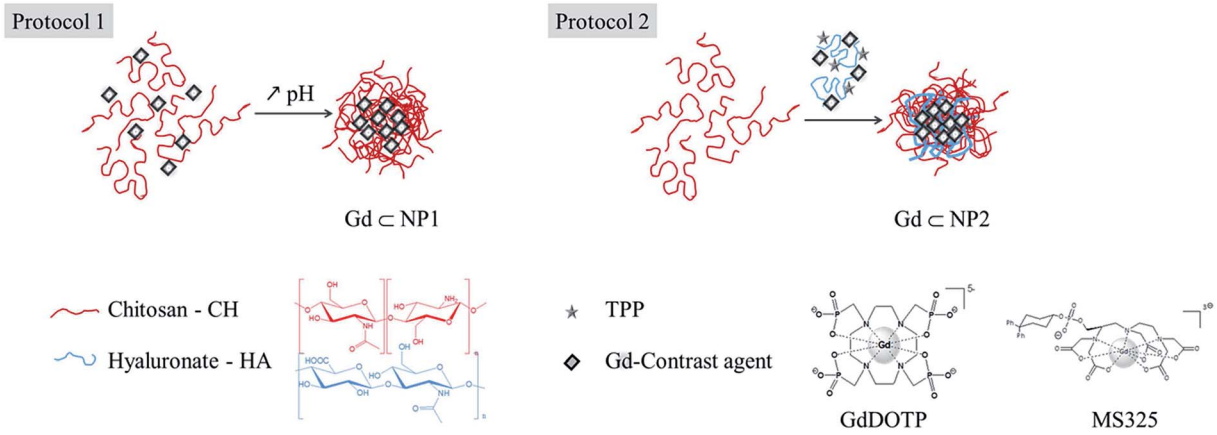

Scheme 1 Nanohydrogel syntheses.

NP size increased. This swelling could be attributed to the hydrogel nature of these nano-objects.[40] Indeed, the nanoparticle water content is at least 90% for each protocol.

The final colloidal suspensions were stable for weeks at room temperature, owing to electrostatic repulsion (ζ-potential ~ 35 mV after dialysis). DLS analysis (Table 1) showed that after dialysis the GdCA⊂NPs exhibited average hydrodynamic diameters between 180 and 620 nm, according to the protocol and the GdCA. AFM images (Fig. 1a and b) highlighted that GdCA⊂NPs were spherical and narrowly monodisperse. The presence of Gd(III) inside the NPs was confirmed by energy-dispersive X-ray spectroscopy on isolated nanoparticles (Fig. 1c and d – for size distribution, see ESI-2†).

GdCA loadings were quantified after nanoparticle purification (Table 1). They were lesser for nanoparticles recovered by dialysis. This indicated that dialysis provoked a partial leakage of the nanoparticle content. However, high levels of Gd chelates per NP were obtained in the range of $1.7–14.5 \times 10^4$ chelates per nanoparticle when the GdCA was GdDOTP or MS325 and in the range of $4.3–52.8 \times 10^4$ chelates per nanoparticle when the GdCA was GdDOTA. These loadings were comparable to those of supramolecular assemblies between Gd chelates, dextran, and poly-β-cyclodextrin.[41] They could be correlated with the existence of efficient hydrophilic interactions between the polymer matrix and entrapped chelates.

GdCA cross-linking abilities and ionic interactions in simple and hybrid polymer networks

In hydrogels constituted of a simple polymer network (GdCA⊂NP1 nanoparticles), the interactions involve the negative charges of GdCAs and the positively charged groups of chitosan.[42] Upon NaOH addition (final pH ~ 5.5), partial deprotonation of chitosan $-NH_3^+$ groups and deprotonation of GdCAs occurred. The ionic interaction between CH and GdCA should then be pH-dependent deprotonation accompanied by partial ionic cross-linking with GdCA. Since the charge of each GdCA should influence the nanoparticle size, the role of GdDOTP as a cross-linking agent was analyzed by comparison with GdDOTA by means of GdCA⊂NP1 sizes before dialysis (and then swelling). Whatever the initial Gd loading, GdDOTP⊂NP1s were more than two times smaller than GdDOTA⊂NP1s (Table 1, entries a, b/g, h). At the beginning of the process, when GdCAs were introduced in the acidic chitosan phase (pH ~ 2.5), they were fully protonated as indicated by acid–base equilibrium calculations ($H_4GdDOTP^-$ and HGdDOTA, see ESI-3†). H_4-$GdDOTP^-$ was two times deprotonated in the pH range 2.5–5.5 while HGdDOTA became one time deprotonated. Accordingly, the cross-linking ability of GdDOTP evolved more favorably as this GdCA behaved as a multivalent counter-ion. This enhanced efficiency was therefore converted into the obtention of smaller

Table 1 Nanoparticle characteristics and Gd(III) loadings of GdDOTP, MS325 and GdDOTA⊂NPs

	GdDOTP⊂NP1		GdDOTP⊂NP2		MS325⊂NP2		GdDOTA⊂NP1		GdDOTA⊂NP2	
Entries	a	b	c	d	e	f	g	h	i	j
$[Gd]_{initial}$ (10^{-4} mol L^{-1})	2.62	6.57	2.70	6.67	2.96	25.9	9.13	19.0	9.01	18.6
$D_H \pm$ sd before dialysis	183 ± 7	158 ± 5	123 ± 2	125 ± 1	116 ± 4	84 ± 3	404 ± 11	447 ± 13	264 ± 4	277 ± 18
After dialysis (nm)	393 ± 5	344 ± 4	185 ± 7	189 ± 3			523 ± 83	618 ± 29	313 ± 20	364 ± 44
DLE (%)	3.95	7.01	1.15	1.85	1.81	19.02	0.46	0.94	0.34	0.36
$[Gd]_{NPs}$ (mM)	0.22	0.40	0.086	0.140	0.14	1.75	0.0245	0.0508	0.0253	0.0269
Y_{Gd} (10^4)[a]	14.2	14.5	1.71	2.40	1.80	6.71	14.9	52.8	4.29	4.49

[a] Y_{Gd} = number of Gd ions per NP: these estimations were based on the measurement of the entrapped gadolinium and on the particle size according to W. J. Rieter, J. S. Kim, K. M. L. Taylor, H. An, W. Lin, T. Tarrant and W. Lin, *Angew. Chem., Int. Ed.*, 2007, **46**, 3680.

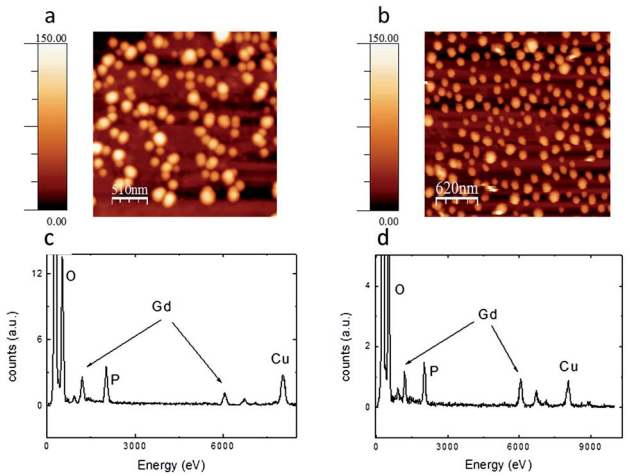

Fig. 1 Fluid tapping mode AFM images of (a) GdDOTP⊂NP2 and (b) MS325⊂NP2. For each image, the color scales represent the *z*-range and are in nm. (c and d) EDXS spectra performed using TEM-EDXS of (c) GdDOTP⊂NP2 and (d) MS325⊂NP2, showing a characteristic Gd signal.

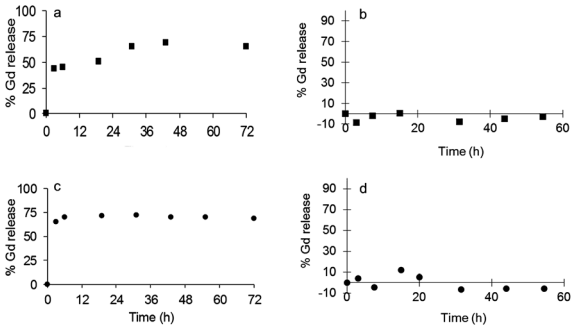

Fig. 2 Release profiles at 37 °C of GdDOTP⊂NP1 in (a) phosphate buffer and (b) simulated plasma, and of GdDOTP ⊂NP2 in (c) phosphate buffer and (d) simulated plasma.

NPs (Table 1, entries a, b/g, and h). In addition, GdCA⊂NP1s containing the higher GdDOTP concentration have smaller sizes (Table 1, entries a/b).

To evaluate the differences between simple and hybrid networks the role of the polyanionic phase in the hydrogel structuration was examined. For this, nanoparticles obtained by both protocols were compared. For a similar initial GdCA loading, GdCA⊂NP2 nanoparticles (Table 1, entries c, d; i, j) were systematically smaller than GdCA⊂NP1 ones (Table 1, entries a, b; g, h). For MS325, no comparison without HA was possible but the NP sizes were similar to the ones obtained for GdDOTP under similar conditions. As previously said, HA is a polyanion and its presence in the gel allowed the development of additional electrostatic interactions between both polymers.[31] The current data suggested that in protocol 2, CH, which is more protonated than in protocol 1, was able to develop intermolecular linkages, at a higher binding ratio than in protocol 1.

To summarize, the smallest NPs were obtained when the two following conditions were satisfied: (i) use of a GdCA which develops optimal interactions with positively charged CH and (ii) use of a second anionic phase which induces the formation of an extended electrostatic network.

GdCA release from NPs

To mimic the behaviour of Gd loaded nanoparticles under *in vitro* conditions, the release of GdDOTP and MS325 from nanocarriers was evaluated at 37 °C under sink conditions in phosphate buffer and in simulated plasma. In phosphate buffer, GdCA release was found to occur much more slowly for Gd⊂NP1 (43% for GdDOTP for the first three hours, Fig. 2a) than for Gd⊂NP2 (65% for GdDOTP (Fig. 2c) and 92% for MS325 for the same period of time (ESI-4†)). These data indicated that the nano-structuration of protocol 1 and 2 hydrogels was different. Gd⊂NP1 nanogels, prepared by CH (and GdCA) deprotonation, may take a loop-shape conformation because of the decrease of amino groups.[43] Gd⊂NP2 nanogels may take a ladder-shape structure because of a higher cross-linking degree.[43] These different structures led to increases of tortuosity and decrease of the gel porosity for Gd⊂NP1 (ref. 43) as compared to Gd⊂NP2 prepared by a fully ionic-crosslinking mechanism.[43] Therefore, Gd⊂NP1 structuration decreased the release rate of GdCAs by limiting the network rearrangement. To have a better insight of Gd⊂NPs under *in vivo* conditions, GdCA leakage from NPs was performed in simulated serum (Fig. 2b and d and ESI-4†). For each Gd⊂NP, Gd release profiles were dramatically different since no significant release was detected for more than two days. The main difference between phosphate buffer and simulated serum is the presence of human serum albumin (HSA 4% (w/v)) in the medium. Since the isoelectric point of HSA is 4.6, at physiological pH, this protein is negatively charged and able to adsorb at the positive surface of the nanogels.[44,45] Therefore, this adsorbed HSA layer could prevent NP disintegration by limiting ion-exchange and then preserving encapsulated GdCAs from release.

Relaxometric studies and 3T imaging

The relaxivities r_i (i = 1 and 2) of MS325⊂NPs and GdDOTP⊂NPs were determined at 20 MHz for nano-objects obtained with each protocol (Table 2). For each sample, the contribution to overall relaxivity from the free GdCA, determined from both its relaxation rate and its concentration in

Table 2 Relaxivities of GdDOTP⊂NPs and MS325⊂NPs at 20 MHz, T = 5 °C and 37 °C

	R_1 (s^{-1} mM^{-1})		r_2 (s^{-1} mM^{-1})	
	37 °C	5 °C	37 °C	5 °C
GdDOTP⊂NP1	41.5 ± 1.6	41.2 ± 1.6	47.6 ± 3.3	48.5 ± 3.8
GdDOTP⊂NP2	98.0 ± 4.9	103.9 ± 4.1	109.5 ± 7.6	122.8 ± 9.8
MS325⊂NP2	52.9 ± 2.6	59.2 ± 2.4	60.9 ± 4.3	63.9 ± 5.1
GdDOTP	4.2 ± 0.2	9.5 ± 0.4	4.48 ± 0.3	11.7 ± 0.9
MS325	5.9 ± 0.3	10.4 ± 0.4	6.8 ± 0.5	11.5 ± 0.9

supernatants, was subtracted (see ESI-5† for calculations). On a per millimolar Gd basis and at 37 °C, MS325⊂NPs presented an r_1 value of 52.9 s^{-1} mM^{-1}. This value was substantially higher than the one of free MS325 (9-fold higher). GdDOTP⊂NPs presented variable r_1 values according to the protocol, between 40 and 100 s^{-1} mM^{-1}, namely 10 to 23-fold higher than for free GdDOTP. The exaltation of relaxivities indicated that in all cases, water access to the GdCA was not restricted by its encapsulation. Similar enhancements were obtained for r_2 values. Interestingly, for GdDOTP⊂NPs, relaxivity values were substantially higher than the ones obtained for GdDOTP loaded nanoparticle-assembled-capsules (NACs).[46] GdDOTP-based NACs are also nanoassemblies constituted of a polymer salt aggregate (cationic polymers such as poly-L-lysine or polyallylamine and multivalent cross-linking anions such as citrate, EDTA and $GdDOTP^{5-}$) inside a silica shell. Except their silica shell, these nanoparticles are comparable to GdDOTP⊂NP1 obtained herein. The better results obtained here for GdDOTP⊂NP1 hydrogels spoke in favour not only for better water permeability relative to what was observed in NACs, but also for good water exchange between the core structure of the hydrogel and the bulk. The temperature dependence of relaxivity could provide insights into the exchange process that dominates in hydrogels. The relaxivity of GdCA⊂NPs remained constant or increased slightly when the temperature decreased (Table 2). This evolution was consistent with intermediate or fast water exchange kinetics for all systems.[46]

The longitudinal relaxation rates were then recorded at 37 °C as a function of resonance frequency and according to hydrogel compositions (Fig. 3a and b). Whatever the GdCA (GdDOTP or MS325), all NMRD profiles exhibited a similar shape with a maximum in relaxivity between 25 and 30 MHz. These results indicated that inside hydrogels GdCA motions were restricted. For GdDOTP⊂NPs, NMRD profiles were also dependent on the hydrogel composition. Indeed, for hydrogels that corresponded to the hybrid polymer network (GdCA⊂NP2), composed of two highly hydrophilic polymers CH and HA, the gain in relaxivity was more important (23-fold higher than for free GdDOTP at 20 MHz) than the one obtained for single polymer network NPs (GdCA⊂NP1, 10-fold higher than for GdDOTP alone at 20 MHz). However, GdDOTP has no inner sphere water molecule.[35] The relaxivity enhancement determined for GdDOTP⊂NP2 could be attributed to a high number of water molecules involved in a network, of H-bonding interactions with the Gd chelates, and then to a strong second sphere contribution. Therefore, in protocol 2 nanohydrogels, not only Gd chelates were confined but also water molecules. Their confinement led to the formation of a highly hydrated environment for the entrapped GdCAs. Moreover, relaxivity enhancements were more important for GdDOTP than for MS325. As previously said, GdDOTP has no inner sphere water molecule while MS325 has one inner sphere molecule.[36] The relaxivity differences observed for GdDOTP⊂NP2 and for MS325⊂NP2 tend to indicate that first sphere relaxation effects have a minor contribution in relaxivity enhancement, which are mainly ruled by the second sphere contribution.

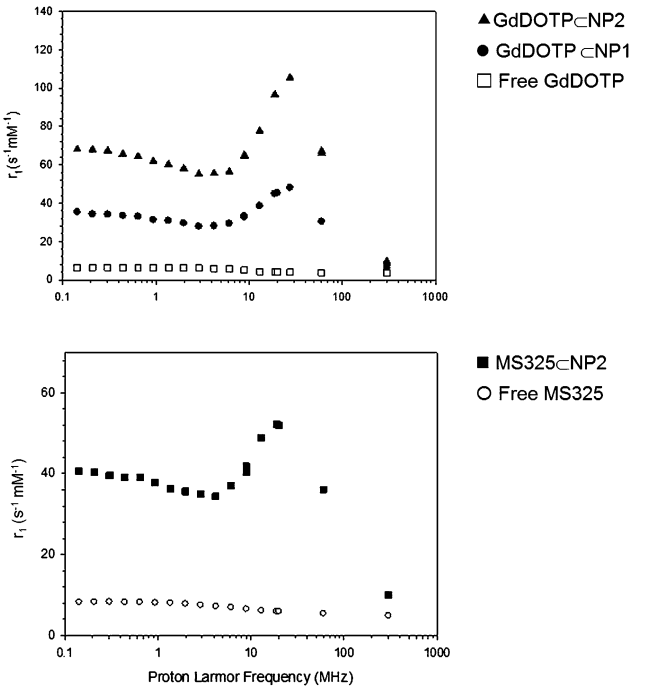

Fig. 3 NMRD relaxivity profiles at 37 °C of (a) GdDOTP⊂NP and (b) MS325⊂NP.

Finally, relaxivity enhancement was dependent on the cross-linking ability of the GdCA. To check this point, the comparison of NMRD profiles of Gd-loaded single polymer network nanoparticles (GdCA⊂NP1), which only differ by the cross-linking ability of the Gd chelate, in the absence of any other influence (namely HA), could be done (see ESI-6†). The gain in relaxivity was lesser for GdDOTP⊂NP1 than for GdDOTA⊂NP1. On a per millimolar Gd basis, GdDOTP⊂NP1 exhibited r_1 values 2-fold smaller than those of GdDOTA⊂NP1 over the entire frequency range. This effect was clearly counterbalanced in GdCA⊂NP2 by the presence of HA. Besides the contribution of HA to the formation of highly crosslinked hydrogels it also provided a supplemental source of hydration for Gd chelates which impacted favourably on the relaxivity.

To demonstrate how relaxivity enhancements were translated into contrast, T_1- and T_2-weighted images of phantoms containing suspensions of GdDOTP⊂NP2 and MS325⊂NP2 obtained by the same protocol were acquired on a 3T clinical imager, with GdDOTP and MS325 as controls (Fig. 4). For the T_1-weighted images, the bright signal enhancement progressively increased with GdDOTP⊂NP2 or MS325⊂NP2 concentrations. Comparison with GdDOTP or MS325 as controls showed that signal enhancement is due to the incorporation of GdCAs within hydrogels. For the T_2-weighted images, under similar conditions signal darkening was observed. Similar contrasts were also obtained for GdDOTP⊂NP1 synthesized *via* protocol 1 (see ESI-7†). All these images were similar to those previously obtained for nanohydrogels loaded with GdDOTA as a contrast agent.[28] They supported not only the relaxometric results but also highlighted the dual T_1/T_2 properties of the GdCA loaded hydrogels.[28]

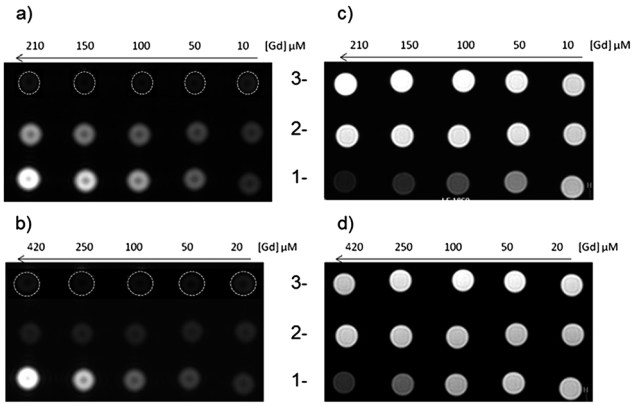

Fig. 4 (a and b) T_1-weighted images of (a) GdDOTP⊂NP2 (line 1), Na_5GdDOTP (line 2), and water (line 3) and (b) MS325⊂NP2 (line 1), MS325 (line 2) and water (line 3). (c and d) T_2-weighted images for the same solutions as in (a) and (b) respectively. Samples imaged at 3 T, 37 °C, and with a standard spin echo (SE) sequence.

Finally, nanoparticle cytotoxicity was tested since it constituted a determinant factor for their *in vivo* use. Primary fibroblast cell viability was monitored using an MTT assay to measure their mitochondrial enzyme activity (ESI-8†).[47] The results of the assay showed that Gd⊂NPs were not toxic to these cells; they were viable even after incubation with a nanoparticle loading of 23 μg mL^{-1} per 5×10^4 fibroblasts for 48 hours.

Conclusions

In conclusion, we have shown that gadolinium loaded chitosan nanohydrogel relaxivities can be tuned according to the gadolinium contrast agent and the hydrogel matrix composition. In the context of ionic gelation, the use of multivalent anionic contrast agent, such as GdDOTP, contributes efficiently to hydrogel cross-linking. Since the high cross-linking degree could limit water access and mobility inside the nanogels, this can be counterbalanced by the association of a second hydrophilic polymer (hyaluronan) and the constitution of high-water content nanoparticles. As an example, GdDOTP⊂NP relaxivities can be increased from 41.5 s^{-1} mM^{-1} (GdDOTP⊂NP1) to 98 s^{-1} mM^{-1} per Gd ion (GdDOTP⊂NP2) while maintaining nanoparticle sizes below 200 nm (GdDOTP⊂NP2). Thus, by encapsulating GdCAs within nanohydrogels, it is both possible to entrap large quantities of Gd centres and to boost the relaxivity of each Gd centre. This could have very interesting implications in the field of targeted MR imaging. Indeed, in this context superparamagnetic iron oxide nanoparticles (SPIO) are often used to track cells or to visualize targets at low concentrations. These nano-objects generate negative contrast which can be a drawback.

Therefore, the high sensitive T_1/T_2 gadolinium probes described herein could constitute an interesting alternative to SPIO. To reach this goal, the functionalization of these nanohydrogels, through the conjugation of active targeting ligands, is currently being investigated.

Experimental

General procedures and materials

Chitosan (low molecular weight, 86% deacetylated) and sodium hyaluronate (extracted from *Streptococcus equi* sp.) were purchased from Sigma (France). Sodium tripolyphosphate was purchased from Acros Organics. Sterile water for injections (Laboratoire Aguettant, Lyon, France) was systematically used for nanoparticle preparation, purification and analysis. DOTP was purchased from Macrocyclics (Dallas, USA) and MS325 (Vasovist, Gadofosveset trisodium) was generously provided by Bayer Schering Pharma. All products were used as received without further purification.

GdDOTP synthesis

66 mg of Gd_2O_3 (0.182 mmol) were added to 200 mg of H_8DOTP (0.365 mmol) dissolved in water (10 mL). After heating the suspension at 95 °C for 24 h, the solution was cooled down and 100 mg of NaOH (2.5 mmol) were added. The solution was then slowly added to 50 mL of acetone under vigorous stirring and the precipitated Na_5GdDOTP was collected by filtration and dried (m = 320 mg, 0.322 mmol, 88% yield). ESI-MS (positive mode, water): m/z calculated for $[C_{12}H_{24}GdN_4Na_5O_{12}P_4–Na]^+$: 835.9, found: 836.0.

Anal calcd for $C_{12}H_{24}GdN_4Na_5O_{12}P_4 \cdot 10H_2O$: C, 14.52%; H, 4.47%; N, 5.64%, found: C, 14.44%; H, 4.11%; N, 5.60%.

Nanogel preparation

Stock solutions of chitosan were prepared by dissolution of CH powder (2.5 m g mL^{-1}) in a 10% citric acid aqueous solution and stirred overnight. Insoluble residues were removed by centrifugation at 3800 rpm for 4 min at room temperature. The Gd nanoparticles were prepared according to the following protocols.

Protocol 1 – single polymer network: GdCA⊂NP1

The gadolinium complex was added to the CH solution (9 mL) and magnetic stirring was maintained for one hour. 1 M NaOH solution was then added dropwise until pH ~5.5 over a 45 min period to obtain a turbid nanosuspension (Tyndall effect).

Protocol 2 – hybrid polymer network: GdCA⊂NP2

Nanoparticles were obtained by an ionotropic gelation process. The polyanion phase, *i.e.* sodium hyaluronate (0.8 mg mL^{-1}) and sodium tripolyphosphate (1.2 mg mL^{-1}) in water (4.5 mL), was added dropwise to the chitosan solution (9 mL) under magnetic stirring. The gadolinium complex was previously dissolved in the polyanion solution. For both protocols, at the end of addition, magnetic stirring was maintained for another 10 min. Unloaded nanoparticles were obtained in the same way, omitting the gadolinium complex.

Nanoparticle purification

Unloaded nanoparticles, GdDOTP⊂NP and GdDOTA⊂NP suspensions (5 mL) were dialyzed three times at room

temperature against 500 mL of water for injections, for 24 h under magnetic stirring (Spectrum, Spectra/Por® 6.0, MWCO 25 kDa) in order to remove citric salts and the non-encapsulated complex. The MS325⊂NP suspensions were purified by gel permeation on a LH-60 Sephadex column equilibrated with water for injections. Fractions corresponding to the particles, macroscopically visible, were collected and pooled together.

The purified suspensions were then concentrated by tangential flow filtration using MicroKros® hollow fiber modules (Spectrum, MicroKros® ME, MWCO 0.1 μm).

Determination of the water content in hydrogels

The water content inside the nanohydrogels was determined using a gravimetric method. A known volume of nanosuspension was centrifuged for 1 h 15 min at 4 °C at 23 200*g* (Beckman Avanti™ J-E Centrifuge, France). The nanoparticle pellet was weighed in a wet state and after lyophilisation (FreeZone6, Labconco). The water content was expressed as:

$$\text{Water content } (\%) = \frac{\left(m^{\text{wet}}_{\text{NP pellet}} - m^{\text{dried}}_{\text{NP pellet}}\right)}{m^{\text{wet}}_{\text{NP pellet}}} \times 100$$

Particle size analysis and zeta-potential measurements

Dynamic light scattering (DLS) was used for measurement of average hydrodynamic diameters (D_H) and polydispersity indices (PdIs) (Malvern Zetasizer Nano-ZS, Malvern Instruments, Worcestershire, UK). Each nanosuspension was analyzed at 20 °C at a scattering angle of 173°, in triplicate for each sample, after 1/20 dilution in water. Pure water was used as a reference dispersing medium. ζ-(zeta) potential data were collected through electrophoretic light scattering at 20 °C, 150 V, in triplicate for each sample, after 1/20 dilution in water. The instrument was calibrated with a Malvern – 68 mV standard before each analysis cycle.

AFM images and TEM-EDXS measurements

The shape and the surface morphology of the nanoparticles were investigated by atomic force microscopy (AFM) (Catalyst, BrükerNano) in tapping mode. Samples were prepared by placing a drop of nanoparticle suspension on a freshly cleaved mica sheet and the experiments were performed in fluid tapping mode under conditions similar to other experiments to keep the integrity of the NPs. AFM images were generated with a scan rate of 1 Hz and 512 lines per image. Experiments were performed at constant room temperature. During the scans, proportional and integral gains were increased to the value just below the feedback started to oscillate. Images were processed only by flattening to remove background slopes. 3D images of isolated NPs (ESI-2†) confirm the shape of the NPs. For each type of NPs, size distributions (ESI-2†) were analyzed using tens of images taken at different positions of the analyzed samples.

A scanning transmission electron microscope (CM30, Philips, Limeil-Brevannes, France) equipped with an EDAX 30 mm^2 Si(Li) R-SUTW detector was used for determining the elemental composition of nanoparticles (TEM-EDXS). In practice, a drop of NP suspension was deposited on a 200-mesh copper grid covered by a collodion/carbon film, air-dried and X-ray spectra were acquired for 100 s at 100 keV by a 24 nm probe in the nanoparticles. The emission spectrum corresponds to the counting of X-rays emitted according to their energy.

Determination of the gadolinium loading by ICP-OES

Gadolinium nanoparticle loading was determined on raw, purified and concentrated nanoparticle suspensions by ICP-OES. The non-encapsulated complexes were separated from the nanoparticles by high speed centrifugation for 1 h 15 min at 4 °C at 23 200*g* (Beckman Avanti™ J-E Centrifuge, France). The nanoparticle pellet was then incubated overnight in a 1 : 3 (v/v) mixture of HCl (37%) and HNO_3 (69%). After the NP destruction, volumetric dilutions were carried out to achieve an appropriate Gd concentration within the working range of the method. Samples were analysed using a Thermo Scientific iCAP 6300 series Duo ICP spectrometer. Counts of Gd were correlated with a Gd calibration curve generated by mixing the $Gd(NO_3)_3$ standard with unloaded nanoparticles incubated under the same acidic conditions.

GdCA loading efficiencies (DLE%) of nanoparticles were calculated by the equation:

$$\text{DLE\%} = \frac{\text{mass of Gd complex in NPs}}{\text{mass of recovered NPs}} \times 100$$

When necessary, the Gd concentration was also determined on nanoparticle supernatants (for relaxivity measurements *vide infra*).

GdCA release from NPs

Release studies were performed both in simulated serum and in phosphate buffer on GdDOTP⊂NP ($[Gd]_{\text{intraNP}}(\text{mM}) = 0.6$ mM) and MS325⊂NP ($[Gd]_{\text{intraNP}}(\text{mM}) = 0.2$ mM), under sink conditions (the volume of the external medium was at least greater than three times that required to form a saturated solution of each GdCA).

For release studies in simulated plasma, Gd⊂NP nanosuspensions (10 mL, $n = 3$ batches) were dispersed in simulated serum (pH 7.4, 90 mL). The release medium was made of KCl (16 mg L^{-1}), NaCl (640 mg L^{-1}), KH_2PO_4 (16 mg L^{-1}) and 4% (w/v) HSA (Human Serum Albumin). All samples were kept at 37 °C under magnetic stirring. At various pre-determined endpoints, aliquots of the release medium were centrifuged (23 200 × *g*, 1 h 15 min, 4 °C) and Gd contents were determined on the pellets.

For release studies in phosphate buffer, 5 mL of NP suspensions were placed in a dialysis membrane (Spectrum, Spectrapor® 6.0, MWCO 24 kDa) and placed at 37 °C against 1.0 L phosphate buffer (pH = 7.4). At given time periods, 200 μL of nanoparticle suspension aliquots were removed, centrifuged at 23 200×*g* for 1 h 15 min, at 4 °C.

The nanoparticle pellets were then incubated overnight in a 1/3 (v/v) mixture of HCl (37%) and HNO_3 (69%). Gd NP loadings

were determined by using an ICP-OES spectrometer as described above. The percentage of released gadolinium chelates was plotted against time. Experiments were performed in quadruplicate.

Relaxivity measurements

T_1 and T_2 measurements at 20 MHz (0.47 T). T_1 and T_2 measurements were performed on a Bruker mq20 Minispec relaxometers (0.47 T) using an inversion recovery pulse sequence. Each sample was analyzed by ICP-OES to take into account the exact Gd(III) concentration. The measurements were performed at two different temperatures. Each temperature was equilibrated and maintained at 5 and 37 °C during the scans. The diamagnetic contribution was measured by recording the longitudinal and transversal times from unloaded nanoparticles at the same NP concentrations than Gd-loaded samples. The inverse of the paramagnetic longitudinal relaxation time ($R_1^{\text{para}} = 1/T_{1\ \text{para}}$, s^{-1}) and paramagnetic transversal relaxation time ($R_2^{\text{para}} = 1/T_{2\ \text{para}}$, s^{-1}) of each sample was calculated according to:

$$R_1^{\text{para}} = (1/T_{i\ \text{para}}) = (1/T_{i\ \text{observed}}) - (1/T_{i\ \text{dia}}) \text{ with } i = 1, 2$$

The relaxivities ($s^{-1}\ mM^{-1}$, $i = 1$ and 2) of the nanoparticles were as follows:

$$r_i(\text{GdCA}\subset\text{NP}) = (R_i^{\text{para}} - ([\text{Gd}]_{\text{free}} \times r_i(\text{GdCA}_{\text{free}}))/[\text{Gd}]_{\text{NPs}}$$

where $[\text{Gd}]_{\text{free}}$ is the concentration of the GdCA in the supernatant, r_i ($\text{GdCA}_{\text{free}}$) is the relaxivity of the free CA, and $[\text{Gd}]_{\text{NPs}}$ is the concentration of Gd entrapped in the NPs.

NMRD profiles. ^{1}H NMRD profiles were measured on a Stelar Spinmaster FFC fast field cycling NMR relaxometer (Stelar, Mede, Pavia, Italy) over a range of magnetic fields extending from 0.24 mT to 0.7 T and corresponding to ^{1}H Larmor frequencies from 0.01 to 30 MHz using 0.6 mL samples in 10 mm o.d. tubes. The temperature was kept constant at 37 °C. Additional relaxation rates at 60 and 300 MHz were obtained with a Bruker Minispec mq60 spectrometer and a Bruker Avance-300 MHz, respectively (Bruker, Karlsruhe, Germany). The diamagnetic contribution of unloaded particles was measured and subtracted from the observed relaxation rates of the Gd-loaded nanoparticles.

MR imaging

MR imaging of NP suspensions were performed using a 3.0 T MRI device (Achieva, Philips Medical Systems, The Netherlands) with an 8 channel head coil. T_1-weighted images were obtained with an axial spin echo T_1 sequence (TR = 160 ms, TE = 8 ms, FOV = 170 × 170 mm, matrix = 192 × 192, slice thickness = 2 mm, excitation number = 1). T_2-weighted images were obtained with an axial turbo spin echo T_2 (TSE multishot) sequence (TR = 5000 ms, TE = 80 ms, FOV = 100 × 100 mm, matrix = 256 × 256, slice thickness = 2 mm, excitation number = 1). For GdDOTP⊂NPs, two series of the NP were tested: NPs issued from protocol 2 were tested in the 10–210 μM range. MS325-loaded NPs were tested in the 20–420 μM range; NPs synthesized by protocol 1 were tested in the 10–420 μM range (ESI†). Previous published data showed that blank NP suspensions induced neither a T_1 nor a T_2 signal enhancement.[28]

In vitro cytotoxicity studies

Primary fibroblasts from rat skin were used as normal, unmodified cells. They were seeded on 96-well plates at a cell density of 1×10^3 cells per well in 100 μL RPMI 1640 supplemented with 10% fetal bovine serum (FBS) and 0.5% streptomycin/penicillin, and grown at 37 °C and 5% CO_2 overnight. The next day, the medium was replaced by either unloaded NPs or Gd⊂NP suspensions diluted in FBS-supplemented DMEN at various concentrations (from 0 to 23.20 μg mL^{-1}). Cells were incubated for another 48 h. The cell viability was then assessed by MTT assay.[47] Untreated cells were taken as a control for 100% viability. The relative cell viability (%) compared to control cells was calculated by ($A_{\text{sample}}/A_{\text{control}}$) × 100. All experiments were repeated in quadruplicate.

Acknowledgements

This work was supported by the ANR (Gadolymph project no. ANR-13-ENM2-0001-01) and PHC TOURNESOL program (project no. 28873 YJ), the Region Champagne Ardenne, the DRRT Champagne Ardenne (through MESR) and the EU-program FEDER (Project NanoBio2, Nano'Mat Platform). The ARC (research contract AUWB-2010—10/15-UMONS-5), the FNRS, the ENCITE program, the COST TD1004 (Theranostics imaging and therapy: an action to develop novel nanosized systems for imaging-guided drug delivery), the UIAP VII program, the European Network of Excellence EMIL (European Molecular Imaging Laboratories) program LSCH-2004-503569 and the Center for Microscopy and Molecular Imaging (CMMI, supported by the European Regional Development Fund and the Walloon Region) are thanked for their support. Isabelle Déchamps-Olivier and Thomas Courant are gratefully acknowledged for their help in transmetallation experiments and determination of the MS325⊂NP2 release profile, respectively.

Notes and references

1 B. Misselwitz, *Eur. J. Radiol.*, 2006, **58**, 375.
2 P. Caravan, *Chem. Soc. Rev.*, 2006, **35**, 512.
3 E. Terreno, D. Delli Castelli, A. Viale and S. Aime, *Chem. Rev.*, 2010, **110**, 3019.
4 P. Hermann, J. Kotek, V. Kubıcek and I. Lukes, *Dalton Trans.*, 2008, **23**, 3027.
5 *The Chemistry of Contrast Agents in Medical Magnetic Resonance Imaging*, ed. A. E.Merbach, L.Helm and E.Toth, Wiley and Sons, Chichester, 2nd edn, 2013.
6 J. M. Idée, M. Port, C. Medina, E. Lancelot, E. Fayoux, S. Ballet and C. Corot, *Toxicology*, 2008, **248**, 77.
7 A. Bertin, A.-I. Michou-Gallani, J. L. Gallani and D. Felder-Flesch, *Toxicol. in Vitro*, 2010, **24**, 1386.

8 S. Aime, D. Delli Castelli, S. Geninatti Crich, E. Gianolio and E. Terreno, *Acc. Chem. Res.*, 2009, **42**, 822.
9 E. Gianolio, R. Stefania, E. Di Gregorio and S. Aime, *Eur. J. Inorg. Chem.*, 2012, 1934.
10 N. Bloembergen and L. O. Morgan, *J. Chem. Phys.*, 1961, **34**, 842.
11 E. Terreno, D. Delli Castelli, A. Viale and S. Aime, *Chem. Rev.*, 2010, **110**, 3019.
12 D. A. Cormode, P. A. Jarzyna, W. J. M. Mulder and Z. A. Fayad, *Adv. Drug Delivery Rev.*, 2010, **62**, 329.
13 M. Botta and L. Tei, *Eur. J. Inorg. Chem.*, 2012, 1945.
14 P. Kesharwani, K. Jain and N. K. Jai, *Prog. Polym. Sci.*, 2014, **39**, 268.
15 D. P. Cormode, P. A. Jarzyna, W. J. M. Mulder and Z. A. Fayad, *Adv. Drug Delivery Rev.*, 2010, **62**, 329.
16 D. Delli Castelli, E. Gianolio, S. Geminatti Crich, E. Terreno and S. Aime, *Coord. Chem. Rev.*, 2008, **252**, 2424 and references therein.
17 A. Accardoa, D. Tesauroa, L. Alojb, C. Pedonea and G. Morelli, *Coord. Chem. Rev.*, 2009, **253**, 2193.
18 J. Della Rocca and W. Lin, *Eur. J. Inorg. Chem.*, 2010, 3725.
19 K. B. Ghiassi, M. M. Olmstead and A. L. Balch, *Dalton Trans.*, 2014, **43**, 7346.
20 H. B. Na, I. C. Song and T. Hyeon, *Adv. Mater.*, 2009, **21**, 2133.
21 (*a*) Z. Liu, F. Pu, J. Liu, L. Jiang, Q. Yuan, Z. Li, J. Ren and X. Qu, *Nanoscale*, 2013, **5**, 4252; (*b*) Z. Liu, F. Pu, S. Huang, Q. Yuan, J. Ren and X. Qu, *Biomaterials*, 2013, **34**, 1712.
22 A. Soleimani, F. Martinez, V. Economopoulos, P. J. Foster, T. J. Scholl and E. R. Gillies, *J. Mater. Chem. B*, 2013, **1**, 1027.
23 J. Lux, M. Chan, L. Vander Elst, E. Schopf, E. Mahmoud, S. Laurent and A. Almutairi, *J. Mater. Chem. B.*, 2013, **1**, 6359.
24 S. Aime, L. Frullano and S. Geninatti Crich, *Angew. Chem., Int. Ed.*, 2002, **41**, 1017.
25 J. A. Peters and K. Djanashvili, *Eur. J. Inorg. Chem.*, 2012, 1961.
26 J. S. Ananta, B. Godin, R. Sethi, L. Moriggi, X. Liu, R. E. Serda, R. Krishnamurthy, R. Muthupillai, R. D. Bolskar, L. Helm, M. Ferrari, L. J. Wilson and P. Decuzzi, *Nat. Nanotechnol.*, 2010, **5**, 815.
27 N. Wartenberg, P. Fries, O. Raccurt, A. Guillermo, D. Imbert and M. Mazzanti, *Chem.–Eur. J.*, 2013, **19**, 6980.
28 T. Courant, V. G. Roullin, C. Cadiou, M. Callewaert, M. C. Andry, C. Portefaix, C. Hoeffel, M. C. de Goltstein, M. Port, S. Laurent, L. Vander Elst, R. Muller, M. Molinari and F. Chuburu, *Angew. Chem., Int. Ed.*, 2012, **51**, 9119.
29 T. Kean and M. Thanou, *Adv. Drug Delivery Rev.*, 2010, **62**, 3.
30 E. J. Oh, K. Park, K. S. Kim, J. Kim, J.-A. Yang, J.-H. Kong, M. Y. Lee, A. S. Hoffman and S. K. Hahn, *J. Controlled Release*, 2010, **141**, 2.
31 H. Yoon, E. J. Dell, J. L. Freyer, L. Campos and W.-D. Jang, *Polymer*, 2014, **55**, 453.
32 X. Z. Shu, K. J. Zhu and W. Song, *Int. J. Pharm.*, 2001, **212**, 19.
33 N. Bhattarai, J. Gunn and M. Zhang, *Adv. Drug Delivery Rev.*, 2010, **62**, 8.
34 J. Berger, M. Reist, J. M. Mayer, O. Felt, N. A. Peppas and R. Gurny, *Eur. J. Pharm. Biopharm.*, 2004, **57**, 19.
35 S. Aime, M. Botta, E. Terreno, P. L. Anelli and F. Uggeri, *Magn. Reson. Med.*, 1993, **30**, 583.
36 P. Caravan, N. J. Cloutier, M. T. Greenfield, S. A. McDermid, S. U. Dunham, J. W. M. Bulte, J. C. Amedio, R. J. Looby, R. M. Supkowski, W. De, W. Horrocks, T. J. McMurry and R. B. Lauffer, *J. Am. Chem. Soc.*, 2002, **124**, 3152.
37 R. A. Carvalho, J. A. Peters and C. F. G. C. Geraldes, *Inorg. Chim. Acta*, 1997, **262**, 167.
38 J. W. Lee, S. Y. Kim, S. S. Kim, Y. M. Lee, K. H. Lee and S. J. Kim, *J. Appl. Polym. Sci.*, 1999, **73**, 113.
39 F. A. Oyarzun-Ampuero, J. Brea, M. I. Loza, D. Torres and M. J. Alonso, *Int. J. Pharm.*, 2009, **381**, 122.
40 N. A. Peppas, J. Z. Hilt, A. Khadenhosseini and R. Langer, *Adv. Mater.*, 2006, **18**, 1345.
41 E. Battistini, E. Gianolio, R. Gref, P. Couvreur, S. Fuzerova, M. Othman, S. Aime, B. Badet and P. Durand, *Chem.–Eur. J.*, 2008, **14**, 4551.
42 X. Z. Shu and K. J. Zhu, *Int. J. Pharm.*, 2002, **233**, 217.
43 F.-L. Mi, S.-S. Shyu, T.-B. Wong, S.-F. Jang, S.-T. Lee and K.-T. Lu, *J. Appl. Polym. Sci.*, 1999, **74**, 1093.
44 N. L. Burn, K. Holmberg and C. Brink, *J. Colloid Interface Sci.*, 1996, **178**, 116.
45 P. Aggarwal, J. B. Hall, C. B. Mc Leland, M. A. Dobrovolskaia and S. E. Mc Neil, *Adv. Drug. Delivery Rev.*, 2009, **61**, 428.
46 S. E. Plush, M. Woods, Y.-F. Zhou, S. B. Kadali, M. S. Wong and A. D. Sherry, *J. Am. Chem. Soc.*, 2009, **131**, 15918.
47 T. Mosmann, *J. Immunol. Methods*, 1983, **65**, 55.